PCCP

PAPER

Cite this: *Phys. Chem. Chem. Phys.*, 2017, **19**, 15562

Initial hydration processes of magnesium chloride: size-selected anion photoelectron spectroscopy and *ab initio* calculations†

Gang Feng,[ab] Cheng-Wen Liu,[c] Zhen Zeng,[a] Gao-Lei Hou,[a] Hong-Guang Xu[ad] and Wei-Jun Zheng *[ad]

Received 5th May 2017,
Accepted 23rd May 2017

DOI: 10.1039/c7cp02965a

rsc.li/pccp

To understand the initial hydration processes of $MgCl_2$, we measured photoelectron spectra of $MgCl_2(H_2O)_n^-$ (n = 0–6) and conducted *ab initio* calculations on $MgCl_2(H_2O)_n^-$ and their neutral counterparts up to n = 7. A dramatic drop in the vertical detachment energy (VDE) was observed upon addition of the first water molecule to bare $MgCl_2^-$. This large variation in VDE can be associated with the charge-transfer-to-solvent (CTTS) effect occurring in the $MgCl_2(H_2O)_n^-$ clusters, as hydration induces transfer of the excess electron of $MgCl_2^-$ to the water molecules. Investigation of the separation of $Cl^- – Mg^{2+}$ ion pair shows that, in $MgCl_2(H_2O)_n^-$ anions, breaking of the first Mg–Cl bond occurs at n = 4, while breaking of the second Mg–Cl bond takes place at n = 6. For neutral $MgCl_2(H_2O)_n$ clusters, breaking of the first Mg–Cl bond starts at n = 7.

1. Introduction

Salt ions can affect water surface tension,[1] water hydrogen bond networks,[2] chemical reaction rates in solutions,[3,4] protein solubility in water,[5–7] and the formation of atmospheric aerosol particles.[8] Therefore, the dissolution of salts plays an important role in chemical reactions, biological systems, and atmospheric chemistry. Many theoretical[9–23] and experimental[24–40] studies have been conducted to understand the microscopic mechanisms of salt dissolution, especially the initial hydration processes of salt ions.

Due to the importance of magnesium in the Hofmeister series, biological systems,[41] energy storage,[42] and atmospheric aerosols,[43,44] the hydration of magnesium ions (Mg^{2+}) and magnesium salts has been investigated extensively, both theoretically and experimentally. The effect of Mg^{2+} on the hydrogen bond network in liquid water have been investigated using X-ray absorption spectroscopy of liquid microjets,[45] Mg^{2+} hydration has been studied using infrared action spectroscopy,[46] and $Mg^{2+}(H_2O)_x$ complexes (x = 2–10) have been studied using threshold collision-induced dissociation experiments and theoretical calculations.[47] Microhydration of $MgNO_3^+$ has been investigated in the gas phase using mass spectrometry, infrared multiple photon dissociation (IRMPD) spectroscopy, and theoretical calculations,[48,49] while $(CH_3COO)Mg^+(H_2O)_n$ (n = 0–4) clusters have been investigated using electrospray ionization mass spectrometry and density functional theory calculations.[50] Furthermore, structure evolution of the $MgSO_4Mg^{2+}$ ternary core ion under hydration has been investigated using size-selected cryogenic vibrational predissociation spectroscopy.[51] Moreover, the formation of contact ion pairs in supersaturated magnesium sulfate solutions[52,53] and magnesium nitrate solutions[54] has been studied using Raman scattering of levitated single droplets.

Magnesium chloride ($MgCl_2$) is commonly used in industry, agriculture, nutrition, and medicine, and is the second most abundant component in sea salt. Although the concentration of $MgCl_2$ in sea salt aerosols is much lower than that of sodium chloride (NaCl), hydrated $MgCl_2$ in sea salt aerosols has been found to contribute significantly to the uptake of atmospheric NO_2, SO_2, and OH, and the production of Cl_2 in the marine boundary layer.[55–59] Magnesium-dependent enzymes are important in the citric acid cycle and glycolytic cycle of higher organisms.[60,61] Mg^{2+} can stabilize the structure of RNA[62] and can catalyze the hydrolysis reaction of Hsc70 ATPase.[63] $MgCl_2$ hydration relates to the biological function of Mg^{2+} ions. To understand the initial hydration processes of $MgCl_2$ and provide useful information

[a] *Beijing National Laboratory for Molecular Sciences, State Key Laboratory of Molecular Reaction Dynamics, Institute of Chemistry, Chinese Academy of Sciences, Beijing 100190, China. E-mail: zhengwj@iccas.ac.cn*
[b] *School of Chemistry and Chemical Engineering, Chongqing University, Chongqing 401331, China*
[c] *Beijing National Laboratory for Molecular Sciences, College of Chemistry and Molecular Engineering, Peking University, Beijing 100871, China*
[d] *University of Chinese Academy of Sciences, Beijing 100049, China*

† Electronic supplementary information (ESI) available: Low-lying isomers of $MgCl_2(H_2O)_n^{-/0}$ (n = 0–6); NPA charge distributions and Cartesian coordinates of the most stable isomers of $MgCl_2(H_2O)_n^{-/0}$ (n = 0–7); comparison of VDEs calculated using different theoretical methods. See DOI: 10.1039/c7cp02965a

regarding the role of hydrated $MgCl_2$ in biological systems and atmospheric chemistry, we have investigated $MgCl_2(H_2O)_n^{-/0}$ clusters using size-selected anion photoelectron spectroscopy and *ab initio* calculations.

2. Experimental and theoretical methods

2.1. Experimental methods

Experiments were conducted on home-made apparatus consisting of a laser vaporization source, a time-of-flight mass spectrometer, and a magnetic-bottle photoelectron spectrometer, as described elsewhere.[64] $MgCl_2(H_2O)_n^-$ clusters were generated in the laser vaporization source, in which a rotating and translating $MgCl_2$ target was ablated with second harmonic (532 nm) light pulses from a nanosecond Nd:YAG laser (Continuum Surelite II-10). Helium carrier gas at $\sim$0.4 MPa backing pressure seeded with water vapor was allowed to expand through a pulsed valve to provide water molecules for the formation of $MgCl_2(H_2O)_n^-$ clusters. The formed clusters were mass-analyzed using time-of-flight mass spectrometry. The most abundant isotopologues in the $MgCl_2(H_2O)_{0\text{-}6}^-$ clusters were mass-selected and decelerated before being photodetached by photons at 532 and 355 nm from another nanosecond Nd:YAG laser (Continuum Surelite II-10). The resulting electrons were energy-analyzed using the magnetic-bottle photoelectron spectrometer. Photoelectron spectra were calibrated with spectra for Cs^- and Bi^- taken under similar conditions. Typical instrumental resolution was $\sim$40 meV for electrons with kinetic energies of 1 eV.

2.2. Theoretical methods

Structures of $MgCl_2(H_2O)_n^-$ (n = 0–7) clusters and their neutral counterparts were optimized with density functional theory employing the ωB97XD functional[65] implemented in the Gaussian 09 program package.[66] Pople-type basis set 6-311++G(d,p)[67] was used for all atoms. The initial structures of n = 1–5 clusters were generated from smaller structures by adding additional water molecules to the Mg atom *via* Mg–O interactions, or to Cl atoms and water molecules *via* OH$\cdots$Cl and OH$\cdots$O hydrogen bonds. The initial structures of the large clusters (n = 6 and 7) were generated using integrated tempering sampling (ITS)[68] molecular dynamics and optimized, first using the classical force field and then with density functional theory at the ωB97XD/6-311++G(d,p) level. For all clusters, the harmonic frequencies were calculated to confirm that the obtained structures were real local minima and to estimate the zero-point vibrational energies. The single point energies of the anionic and neutral clusters with n = 0–6 were also calculated by employing coupled-cluster theory, including single, double, and non-iterative triple excitations (CCSD(T))[69] based on structures optimized at the ωB97XD/6-311++G(d,p) level. Natural population analysis (NPA)[70] was performed using NBO version 3.1,[71] as implemented in the Gaussian 09 package.

We also conducted calculations employing the LC-ωPBE and CAM-B3LYP functionals to check the performance of the ωB97XD functional. The results from the LC-ωPBE and CAM-B3LYP functionals were similar to those from the ωB97XD method. However, the ωB97XD method results were in slightly better agreement with experimental values (Fig. S1, ESI†).

3. Experimental results

Photoelectron spectra of $MgCl_2(H_2O)_n^-$ (n = 0–6) clusters were recorded with photons at 532 and 355 nm, as shown in Fig. 1. The vertical detachment energies (VDEs) of these clusters were measured from the peak apex of the corresponding spectrum, while adiabatic detachment energies (ADEs) were estimated by adding the instrument resolution to the electron binding energy (EBE) at the crossing point of the leading edges of the first peak and baseline. The VDEs and ADEs determined are summarized in Table 1. Each spectrum showed only one dominant broad peak, except that for $MgCl_2(H_2O)^-$, which showed a major peak centered at 0.84 eV (A) and two additional peaks at 1.30 eV (B) and 2.10 eV (C), respectively. In the 355 nm

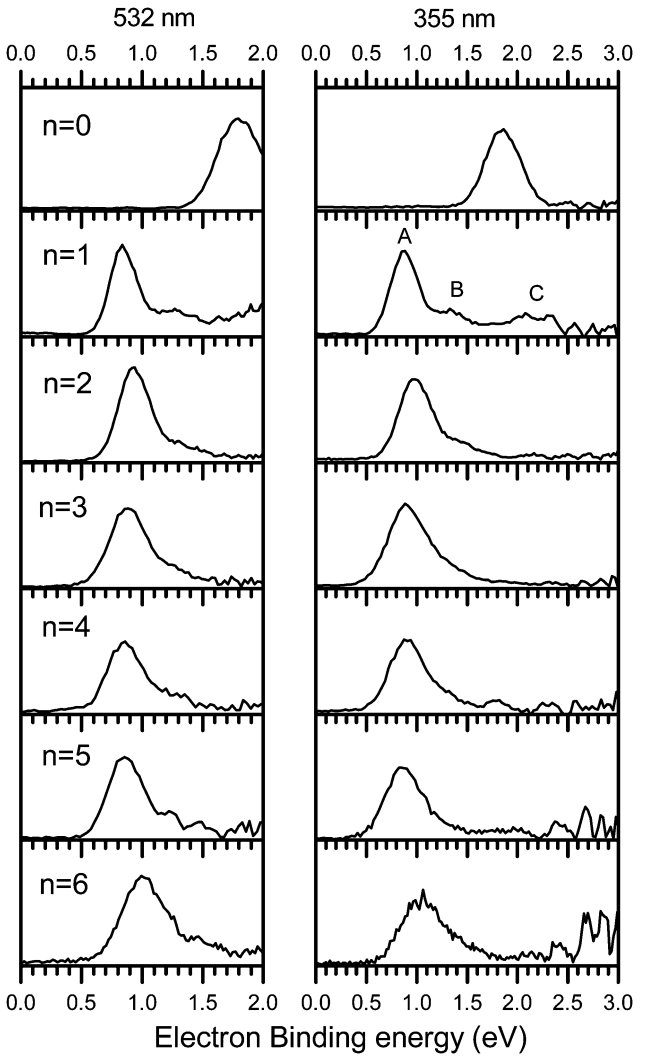

Fig. 1 Photoelectron spectra of $MgCl_2(H_2O)_n^-$ (n = 0–6) recorded using photons at 532 and 355 nm.

Table 1 Low energy isomers of $MgCl_2(H_2O)_n^-$ (n = 0–6) and a comparison of theoretical VDEs and ADEs with experimental values. ΔE, VDE, and ADE were obtained at the CCSD(T)//ωB97XD/6-311++G(d,p) level, and ΔE and ADE were corrected using zero-point energies calculated at the ωB97XD/6-311++G(d,p) level

			Theoretical		Experimental	
n	Isomer	ΔE (eV)	VDE (eV)	ADE (eV)	VDE (eV)	ADE[a] (eV)
0	**0a**	0.000	1.78	0.96	1.80	1.42
1	**1a**	0.000	0.63	0.48	0.84	0.63
	1b	0.117	1.66	0.36	1.30	
	1c	0.121	2.24	1.43	2.10	
	1d	0.222	2.20	0.26		
2	**2a**	0.000	0.84	0.36	0.92	0.65
	2b	0.167	0.45	0.20		
	2c	0.351	1.67	0.35		
	2d	0.387	2.12	0.84		
3	**3a**	0.000	0.82	0.28	0.88	0.58
	3b	0.009	0.67	0.18		
	3c	0.019	0.94	0.28		
	3d	0.040	0.66	0.23		
4	**4a**	0.000	0.81	0.43	0.86	0.56
	4b	0.041	0.68	0.41		
	4c	0.084	0.75	0.17		
	4d	0.122	2.91	0.82		
5	**5a**	0.000	0.80	0.35	0.86	0.56
	5b	0.070	0.72	0.31		
	5c	0.189	0.72	0.27		
	5d	0.189	0.67	0.41		
6	**6a**	0.00	1.08	0.64	1.01	0.62
	6b	0.017	1.32	0.29		
	6c	0.021	0.92	0.35		
	6d	0.043	0.77	0.39		

[a] Experimental ADEs may not represent real ADEs due to possible significant structural changes between anions and neutral clusters. Therefore, the experimental ADEs were not used to verify theoretical calculations.

spectra of $MgCl_2(H_2O)_5^-$ and $MgCl_2(H_2O)_6^-$, signals in the range 2.5–3.0 eV were due to background noise or impurities. Comparison of the main peaks in the spectra of $MgCl_2(H_2O)_n^-$ showed that the VDE dropped abruptly from 1.80 eV to 0.84 eV with the addition of the first water molecule to bare $MgCl_2^-$, increased again to 0.92 eV in $MgCl_2(H_2O)_2^-$, then decreased slightly to 0.88, 0.86, and 0.86 eV for $MgCl_2(H_2O)_n^-$ with n = 3–5, respectively, and finally increased again to 1.01 eV for $MgCl_2(H_2O)_6^-$.

4. Theoretical results

Typical low-lying energy isomers of the $MgCl_2(H_2O)_n^-$ (n = 0–6) clusters and their neutral counterparts are shown in Fig. 2 and 3, respectively. The calculated relative energies, VDEs, and ADEs of $MgCl_2(H_2O)_n^-$ (n = 0–6) are listed in Table 1, along with experimental VDEs and ADEs for comparison.

Bare $MgCl_2^-$ (**0a**) had a bent structure with a ∠ClMgCl angle of 118° and Mg–Cl bond lengths of about 2.34 Å. The theoretical VDE for bare $MgCl_2^-$ (1.78 eV) was in good agreement with the experimental value (1.80 eV).

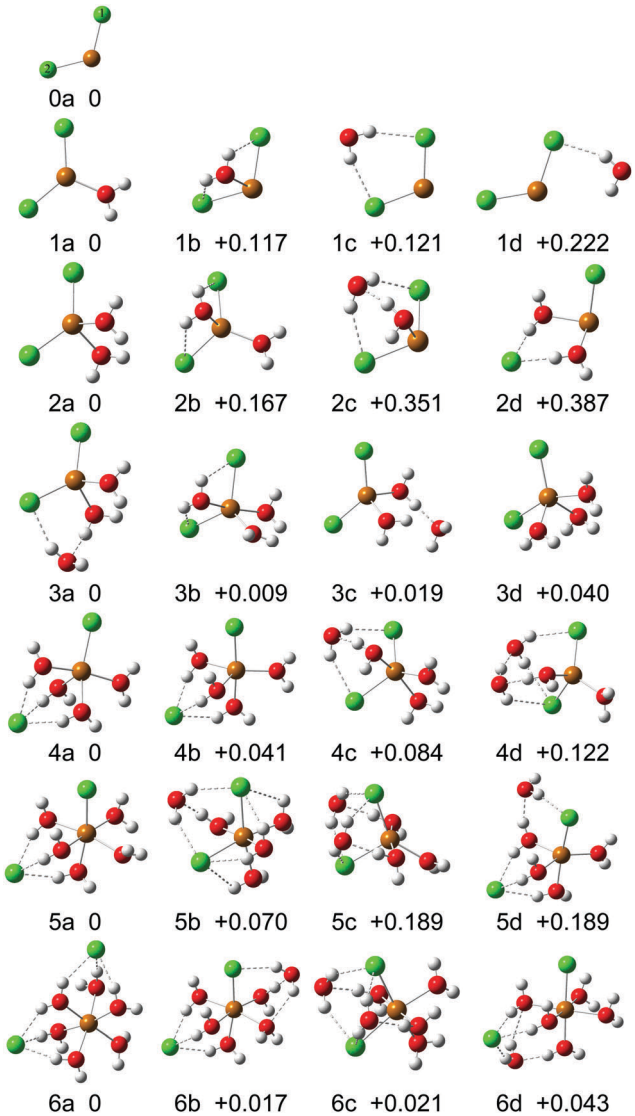

Fig. 2 Typical low-lying isomers of $MgCl_2(H_2O)_n^-$ (n = 0–6) optimized at the ωB97XD/6-311++G(d,p) level of theory. Relative energies (eV) were obtained at the CCSD(T)//ωB97XD/6-311++G(d,p) level of theory and corrected using zero-point energies calculated at the ωB97XD/6-311++G(d,p) level.

Our calculations found four low-lying isomers for $MgCl_2(H_2O)^-$, in which H_2O and $MgCl_2^-$ were arranged head-to-head (**1a**), parallel (**1b**), tail-to-tail (**1c**), and side-by-side (**1d**), respectively. Isomer **1a** had a quasi-planar structure formed by adding H_2O to $MgCl_2^-$ *via* an Mg–O interaction. Isomer **1b** had H_2O connected to $MgCl_2^-$ *via* one Mg–O interaction and two OH···Cl hydrogen bonds, in which the HOH plane was above and almost parallel to that of ClMgCl. Isomer **1c** had a planar structure with H_2O and $MgCl_2$ interacting through two OH···Cl hydrogen bonds. In isomer **1d**, the H_2O approached the bent $MgCl_2$ from one side and formed an OH···Cl hydrogen bond. The ∠ClMgCl angles in isomers **1a**, **1b**, **1c**, and **1d** were 128°, 112°, 113°, and 118°, respectively, because they interacted with H_2O differently. Isomers **1b** and **1c** were higher in energy than **1a** by 0.117 and 0.121 eV, respectively. The theoretical VDE of **1a** (0.63 eV) agreed with the main peak at 0.84 eV (A) in the experimental spectrum.

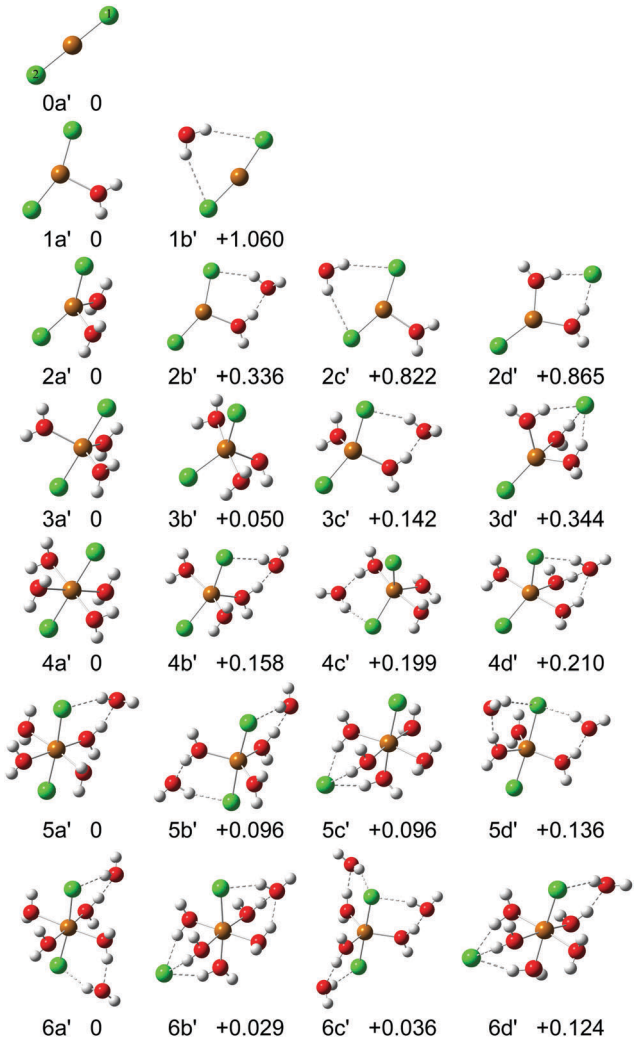

Fig. 3 Typical low-lying isomers of neutral $MgCl_2(H_2O)_n$ (n = 0–6) obtained at the ωB97XD/6-311++G(d,p) level of theory. Relative energies (eV) were obtained at the CCSD(T)//ωB97XD/6-311++G(d,p) level of theory and corrected using zero-point energies calculated at the ωB97XD/6-311++G(d,p) level.

The theoretical VDEs of isomers **1b** and **1c** (1.66 and 2.24 eV) agreed with the small peaks at 1.30 eV (B) and 2.10 eV (C) in the experimental spectrum. Therefore, isomers **1a**, **1b**, and **1c** coexisted in the experiment. Isomer **1d** was higher in energy than isomer **1a** by 0.222 eV, so its contribution to the experimental spectrum might have been negligible.

The VDEs calculated for the most stable isomers of $MgCl_2(H_2O)_n^-$ (n = 2–6) were all in good agreement with experimental values (Table 1). The most stable isomer of $MgCl_2(H_2O)_2^-$ (**2a**) had two water molecules connecting to the Mg atom *via* their O atoms, while that of $MgCl_2(H_2O)_3^-$ (**3a**) was derived from isomer **2a**, with the third H_2O connected to one of the Cl atoms *via* an OH···Cl hydrogen bond and forming an O···HO hydrogen bond with a neighboring H_2O. The ∠ClMgCl angles in isomers **2a** and **3a** were 128° and 126°, respectively, which were similar to that in $MgCl_2(H_2O)^-$ (**1a**). In the most stable isomer of $MgCl_2(H_2O)_4^-$ (**4a**), four water molecules were coordinated to the Mg atom through their O atoms, with three inserted into a Mg–Cl bond to form OH···Cl hydrogen bonds with one Cl atom. The ∠ClMgCl angle had changed to ~140°. Similarly, the most stable isomer of $MgCl_2(H_2O)_5^-$ (**5a**) had five water molecules coordinated with the Mg atom *via* their O atoms, with three of them also inserted into a Mg–Cl bond to form OH···Cl hydrogen bonds with one Cl atom. In both $MgCl_2(H_2O)_4^-$ and $MgCl_2(H_2O)_5^-$, an Mg–Cl bond was broken due to the insertion of three water molecules into it. In the most stable isomer of $MgCl_2(H_2O)_6^-$ (**6a**), six water molecules interacted directly with Mg *via* their O atoms, and each Cl atom interacted with three water molecules *via* hydrogen bonds. Therefore, two Mg–Cl bonds were broken for n = 6, resulting from the insertion of three water molecules into each Mg–Cl bond.

As shown in Fig. 3, the neutral $MgCl_2(H_2O)_n$ clusters preferred larger ∠ClMgCl angles compared with their anionic counterparts. The energy differences between the second and first isomers of the neutral clusters were larger than those of the anions. Unlike the bent structure of the $MgCl_2^-$ anion, neutral $MgCl_2$ (**0a′**) had a linear structure (∠ClMgCl = 180°) with Mg–Cl bond lengths of 2.19 Å, which was consistent with experimental data (2.179 Å) from the previous electron diffraction experiment.[72] The global minimum structure of neutral $MgCl_2(H_2O)$ (**1a′**) had a head-to-head arrangement, with H_2O interacting with the Mg atom *via* its O atom. The second isomer (**1b′**) had a tail-to-tail arrangement, and was much higher in energy than **1a′** by 1.06 eV. The ∠ClMgCl angles in isomers **1a′** and **1b′** were 157° and 169°, respectively, which were much larger than those in the anionic counterparts (**1a** and **1c**). The most stable structure of $MgCl_2(H_2O)_2$ (**2a′**) had a bent Cl–Mg–Cl (∠ClMgCl = 150°) with two water molecules connected to the Mg atom through their O atoms. The most stable structure of $MgCl_2(H_2O)_3$ (**3a′**) had a linear Cl–Mg–Cl arrangement with three water molecules coordinated to the Mg atom through their O atoms. The most stable isomer of $MgCl_2(H_2O)_4$ (**4a′**) had a quasi-linear Cl–Mg–Cl structure, with the Mg atom fully coordinated with two Cl atoms and four water molecules. The most stable structures of $MgCl_2(H_2O)_5$ (**5a′**) and $MgCl_2(H_2O)_6$ (**6a′**) were derived from **4a′**, in which the fifth and sixth water molecules each interacted with a Cl atom and a neighboring water molecule *via* hydrogen bonds. No Mg–Cl bond was broken in the neutral $MgCl_2(H_2O)_n$ clusters of $n \leq 6$.

To better understand the microscopic hydration of $MgCl_2$, we calculated the structures of $MgCl_2(H_2O)_7^-$ and its neutral counterpart, as shown in Fig. 4. The low-lying isomers of the $MgCl_2(H_2O)_7^-$ anion were derived from the most stable isomer of $MgCl_2(H_2O)_6^-$ (**6a**) with the Mg atom fully coordinated by six water molecules and the seventh water molecule added into the second hydration shell. The two Mg–Cl distances in $MgCl_2(H_2O)_7^-$ were slightly elongated compared with those in $MgCl_2(H_2O)_6^-$ (**6a**). The low-lying isomers of neutral $MgCl_2(H_2O)_7$ (**7a′**, **7b′**, and **7d′**) were essentially characterized as Mg^{2+} coordinated by one Cl atom and five water molecules, with the sixth and seventh water molecules in the second hydration shell. Furthermore, an isomer similar to those of the $MgCl_2(H_2O)_7^-$ anion was also found for neutral $MgCl_2(H_2O)_7$, namely **7c′**. Isomer **7c′** was higher in

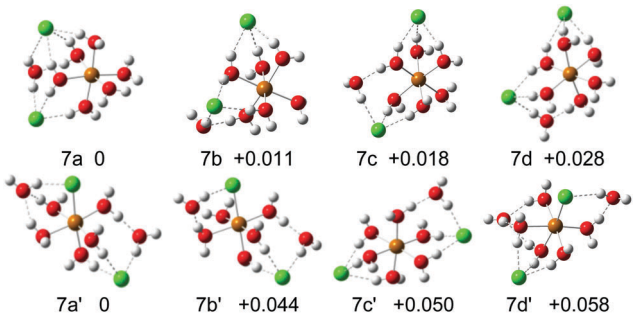

Fig. 4 Typical low-lying isomers of $MgCl_2(H_2O)_7^-$ (**7a–7d**) and $MgCl_2(H_2O)_7$ (**7a′–7d′**) obtained at the ωB97XD/6-311++G(d,p) level of theory. Relative energies are in eV.

Table 2 Mg–Cl distances (Å) in the most stable isomers of anionic and neutral $MgCl_2(H_2O)_n$ (n = 0–7) clusters

	Anion		Neutral	
n	Mg–Cl (1)	Mg–Cl (2)	Mg–Cl (1)	Mg–Cl (2)
0	2.34	2.34	2.19	2.19
1	2.27	2.27	2.22	2.22
2	2.30	2.30	2.26	2.26
3	2.29	2.33	2.35	2.35
4	2.33	3.82	2.38	2.38
5	2.43	3.86	2.41	2.41
6	3.79	3.82	2.43	2.45
7	3.82	4.16	2.47	4.03

energy than **7a′** by 0.050 eV, and had the Mg^{2+} ion fully coordinated by six water molecules, with the seventh water molecule added into the second shell.

Table 2 shows variations in Mg–Cl distances in the most stable isomers of $MgCl_2(H_2O)_n^-$ (n = 0–7) clusters and their neutral counterparts. In the $MgCl_2(H_2O)_n^-$ anion, the Mg–Cl distances decreased from 2.34 to 2.27 Å when n increased from 0 to 1 because the excess electron was delocalized to the water molecule, which enhanced the Coulomb attraction between Mg^{2+} and the Cl^- ions. The Mg–Cl distances then increased slightly at n = 2 and 3. For n = 4 and 5, one of the Mg–Cl bonds was broken, resulting in their corresponding Mg–Cl distances increasing significantly to 3.82 and 3.86 Å, respectively. At n = 6, the two Mg–Cl distances increased to 3.79 and 3.82 Å due to two Mg–Cl bonds breaking. The two Mg–Cl distances in $MgCl_2(H_2O)_7^-$ increased slightly, to 3.82 and 4.16 Å, compared with those in $MgCl_2(H_2O)_6^-$. For the neutral $MgCl_2(H_2O)_n$ clusters, the Mg–Cl distances increased slightly from 2.19 to 2.45 Å with increasing number of water molecules from 0 to 6, then, at n = 7, one of the Mg–Cl distances was elongated abruptly to 4.03 Å, while the other Mg–Cl bond length increased slightly to 2.47 Å.

5. Discussion

We conducted natural population analysis (NPA) on the charge distributions of the most stable structures for anionic and neutral $MgCl_2(H_2O)_{0-7}$ clusters (Table 3 and Fig. 5). The charges

Table 3 NPA charge distributions (e) in the most stable isomers of anionic and neutral $MgCl_2(H_2O)_n$ (n = 0–7) clusters

	Anion				Neutral			
n	Mg	Cl (1)	Cl (2)	nH_2O	Mg	Cl (1)	Cl (2)	nH_2O
0	+0.60	−0.80	−0.80	—	+1.42	−0.71	−0.71	—
1	+1.24	−0.75	−0.75	−0.74	+1.36	−0.71	−0.71	+0.06
2	+1.22	−0.75	−0.75	−0.72	+1.27	−0.72	−0.72	+0.17
3	+1.22	−0.74	−0.74	−0.74	+1.24	−0.74	−0.74	+0.24
4	+1.29	−0.75	−0.83	−0.71	+1.22	−0.74	−0.74	+0.26
5	+1.20	−0.77	−0.84	−0.59	+1.14	−0.73	−0.75	+0.34
6	+1.30	−0.84	−0.84	−0.62	+1.16	−0.74	−0.74	+0.32
7	+1.32	−0.86	−0.82	−0.64	+1.28	−0.74	−0.78	+0.44

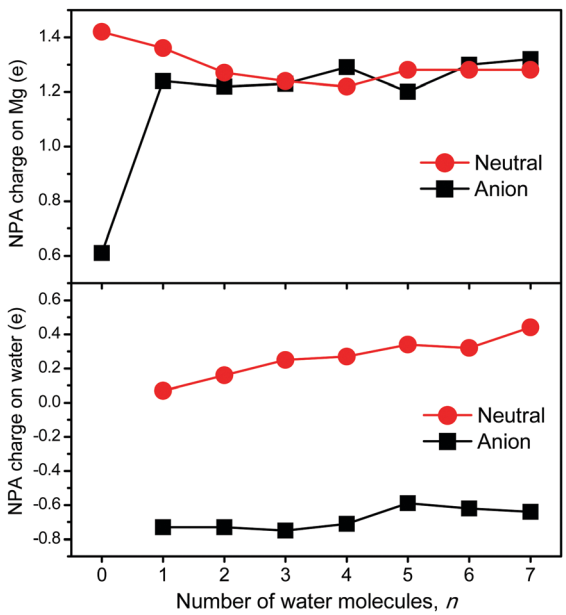

Fig. 5 NPA charge distributions on Mg atom and water molecules in the most stable structures of anionic and neutral $MgCl_2(H_2O)_n$ (n = 0–7) clusters.

on the two Cl atoms were very similar in both anionic and neutral $MgCl_2(H_2O)_{0-7}$ clusters. The charge on the Mg atom in $MgCl_2^-$ was +0.60 e, which was much smaller than that in neutral $MgCl_2$ (+1.42 e), indicating that the excess electron in $MgCl_2^-$ was mainly localized on the Mg atom. Upon addition of the first H_2O molecule, the charge on the Mg atom in $MgCl_2(H_2O)^-$ increased dramatically to +1.24 e, with the H_2O molecule carrying a charge of −0.74 e. Similarly, the charges on the Mg atom of $MgCl_2(H_2O)_{2-7}^-$ were in the range +1.20 to +1.32 e, and their water molecules carried negative charges in the range −0.59 to −0.74 e. In the neutral $MgCl_2(H_2O)_{1-7}$ clusters, the charges on the Mg atom ranged from +1.22 to +1.36 e and the water molecules carried positive charges ranging from +0.06 to +0.44 e. Interestingly, both the anionic and neutral $MgCl_2(H_2O)_n$ clusters showed charge-transfer-to-solvent (CTTS) behavior, in which the negative charge was shifted to the water molecules in the anions, while positive charge was shifted to the water molecules in the neutral clusters. Therefore, the Mg atom retained its charge state in both anionic and neutral

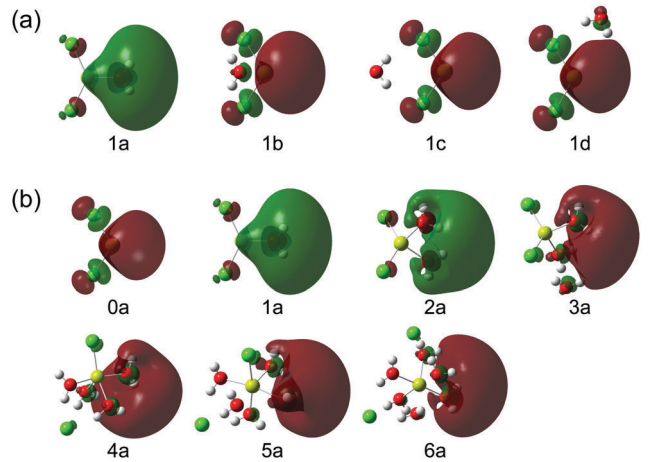

Fig. 6 Diagrams of singly occupied molecular orbitals (SOMOs) in (a) the low-lying isomers of $MgCl_2(H_2O)^-$ and (b) the most stable structures of $MgCl_2(H_2O)_n^-$ (n = 0–6).

$MgCl_2(H_2O)_n$ clusters, whereas variations in charge between the anionic and neutral states of $MgCl_2(H_2O)_n$ clusters were mainly present in the water molecules rather than on the Mg atom. The charge dispersion behavior in the neutral $MgCl_2(H_2O)_{1-7}$ clusters was consistent with that of the bulk[45] and $Mg^{2+}(H_2O)_n$ clusters.[73] The different charge distributions between anions and neutrals also explained the decrease in Mg–Cl bond lengths in the anions and the increase in Mg–Cl bond lengths in the neutral clusters at n = 1, because addition of the first water molecule enhanced the Mg^{2+}–Cl^- Coulomb attraction in the $MgCl_2^-$ anion, but weakened it in neutral $MgCl_2$.

Fig. 6 shows singly occupied molecular orbitals (SOMOs) in the low-lying isomers of $MgCl_2(H_2O)^-$ and the most stable structures of $MgCl_2(H_2O)_n^-$ (n = 0–6). First, we compared the SOMOs in different isomers of $MgCl_2(H_2O)^-$ (**1a**, **1b**, **1c**, and **1d**). The SOMO was found to be mainly localized on the water molecule in isomer **1a**, and dispersed slightly from the Mg atom toward H_2O in isomer **1b**. However, it remained localized on the Mg atom in isomers **1c** and **1d**. These results showed that the shift of the SOMO (or the excess electron) was strongly related to the different types of $MgCl_2^-$–water interaction. Next, we looked at the evolution of SOMO with an increasing number of water molecules. The SOMOs of the most stable structures of $MgCl_2(H_2O)_n^-$ (n = 0–6) showed that the SOMO was mainly located on the Mg atom for bare $MgCl_2^-$ (n = 0), but had largely shifted to the water molecules at n = 1–6. This change in SOMO with the number of water molecules was in good agreement with the charge distribution analysis. The dispersion of the SOMO and the excess electron onto water molecules explained the dramatic drop in VDE for $MgCl_2(H_2O)^-$ (**1a**) compared with that of bare $MgCl_2^-$ (**0a**). Furthermore, the similarity in charge distributions and SOMOs of $MgCl_2(H_2O)_{1-6}^-$ might explain why the variation in VDE from n = 1 to 6 was much smaller than that from n = 0 to 1. It should be noted that there are many literature reports concerning hydrated magnesium species containing excess or unpaired electrons, and solvation-induced electron transfer in $Mg^+(H_2O)_n$ clusters.[74–83] In this work, the shift in the SOMO (or excess electron) from the Mg atom toward the water molecules in $MgCl_2(H_2O)^-$ clusters confirmed the results for the $Mg^+(H_2O)_n$ system in previous studies.

Our previous studies showed that at least nine water molecules were needed to separate a Na^+–Cl^- ion pair.[84] Herein, for $MgCl_2$, the first Mg–Cl bond could be broken upon the addition of seven water molecules, resulting in one of the Cl^- anions being dissociated from $MgCl_2$ and moving to the surface region of the cluster. Using the single point energies for the most stable isomers of $NaCl(H_2O)_{1-6}$ in our previous work[84] and those of $MgCl_2(H_2O)_{1-6}$ in this work, we can obtain water binding energies (WBEs) for stepwise hydration, where WBE is defined as:

$$\mathrm{WBE} = E[\mathrm{Salt}(H_2O)_{n-1}] + E(H_2O) - E[\mathrm{Salt}(H_2O)_n]\ (\mathrm{Salt} = \mathrm{NaCl}, MgCl_2)$$

The WBEs of $NaCl(H_2O)_n$ with n = 1–6 were calculated as 70, 66, 58, 48, 46, and 44 kJ mol^{-1}, respectively, while those of $MgCl_2(H_2O)_n$ with n = 1–6 were calculated as 108, 97, 75, 78, 59, and 64 kJ mol^{-1}, respectively. The WBEs of the $MgCl_2(H_2O)_n$ clusters were larger than those of $NaCl(H_2O)_n$ by approximately 30–60%, implying that hydrating $MgCl_2$ was much easier than hydrating NaCl in humid air. It has been reported that Cl^- anions at the surface region of aerosols are the major participants in reactions related to the uptake of gas phase OH, SO_2, and NO_2,[55,57] and the formation of molecular chlorine from the photolysis of ozone and aqueous sea-salt particles.[85] Our findings, showing that it is easier to hydrate $MgCl_2$ and produce isolated surface Cl^- anions using less water compared with NaCl, might explain why $MgCl_2$ plays an important role in the above reactions in atmospheric aerosols. The large WBEs of $MgCl_2(H_2O)_n$ clusters implied that $MgCl_2$ hydration in water clusters reflects the behavior of $MgCl_2$ salt in bulk solution to some extent, and is consistent with the gas-phase behavior of hydrated salts and the precipitation of salts in bulk identified in previous studies.[86,87]

6. Conclusions

We investigated $MgCl_2(H_2O)_n^{-/0}$ clusters using size-selected anion photoelectron spectroscopy and *ab initio* calculations. The results showed that breaking of one Mg–Cl bond started at n = 4 and breaking of two Mg–Cl bonds started at n = 6 for the $MgCl_2(H_2O)_n^-$ anions. For neutral $MgCl_2(H_2O)_n$ clusters, breaking of the first Mg–Cl bond occurred at n = 7. Charge-transfer-to-solvent (CTTS) behavior was observed in both anionic and neutral $MgCl_2(H_2O)_n$ clusters. The Mg atom retained its charge state by transferring the negative charge to water in the anionic clusters, while transferring positive charge to water in the neutral clusters. Consequently, variations in charge between the anionic and neutral states of $MgCl_2(H_2O)_n$ clusters were mainly exhibited on the water molecules.

Acknowledgements

This work was supported by the National Natural Science Foundation of China (Grant No. 21403249 and 21543007) and the Beijing National Laboratory for Molecular Sciences.

Quantum calculations were conducted on the ScGrid of the Supercomputing Center, Computer Network Information Center of Chinese Academy of Sciences.

References

1 P. B. Petersen and R. J. Saykally, *Annu. Rev. Phys. Chem.*, 2006, **57**, 333–364.
2 Y. Marcus, *Chem. Rev.*, 2009, **109**, 1346–1370.
3 E. Pines, D. Huppert and N. Agmon, *J. Phys. Chem.*, 1991, **95**, 666–674.
4 A. Kumar and S. S. Pawar, *Tetrahedron*, 2003, **59**, 5019–5026.
5 K. D. Collins, G. W. Neilson and J. E. Enderby, *Biophys. Chem.*, 2007, **128**, 95–104.
6 D. J. Tobias and J. C. Hemminger, *Science*, 2008, **319**, 1197–1198.
7 W. J. Xie and Y. Q. Gao, *J. Phys. Chem. Lett.*, 2013, **4**, 4247–4252.
8 U. Pöschl, *Angew. Chem., Int. Ed.*, 2005, **44**, 7520–7540.
9 D. E. Woon and T. H. Dunning, Jr., *J. Am. Chem. Soc.*, 1995, **117**, 1090–1097.
10 G. H. Peslherbe, B. M. Ladanyi and J. T. Hynes, *J. Phys. Chem. A*, 1998, **102**, 4100–4110.
11 C. P. Petersen and M. S. Gordon, *J. Phys. Chem. A*, 1999, **103**, 4162–4166.
12 G. H. Peslherbe, B. M. Ladanyi and J. T. Hynes, *J. Phys. Chem. A*, 2000, **104**, 4533–4548.
13 G. H. Peslherbe, B. M. Ladanyi and J. T. Hynes, *Chem. Phys.*, 2000, **258**, 201–224.
14 P. Jungwirth, *J. Phys. Chem. A*, 2000, **104**, 145–148.
15 S. Yamabe, H. Kouno and K. Matsumura, *J. Phys. Chem. B*, 2000, **104**, 10242–10252.
16 P. Jungwirth and D. J. Tobias, *J. Phys. Chem. B*, 2001, **105**, 10468–10472.
17 S. Godinho, P. C. do Couto and B. J. C. Cabral, *Chem. Phys. Lett.*, 2006, **419**, 340–345.
18 A. C. Olleta, H. M. Lee and K. S. Kim, *J. Chem. Phys.*, 2006, **124**, 024321.
19 A. C. Olleta, H. M. Lee and K. S. Kim, *J. Chem. Phys.*, 2007, **126**, 144311.
20 G. Sciaini, R. Fernandez-Prini, D. A. Estrin and E. Marceca, *J. Chem. Phys.*, 2007, **126**, 174504.
21 T. Jin, B. Zhang, J. Song, L. Jiang, Y. Qiu and W. Zhuang, *J. Phys. Chem. A*, 2014, **118**, 9157–9162.
22 J. Timko, D. Bucher and S. Kuyucak, *J. Chem. Phys.*, 2010, **132**, 114510.
23 C. W. Liu, F. Wang, L. Yang, X. Z. Li, W. J. Zheng and Y. Q. Gao, *J. Phys. Chem. B*, 2014, **118**, 743–751.
24 B. S. Ault, *J. Am. Chem. Soc.*, 1978, **100**, 2426–2433.
25 G. Gregoire, M. Mons, C. Dedonder-Lardeux and C. Jouvet, *Eur. Phys. J. D*, 1998, **1**, 5–7.
26 X. B. Wang, C. F. Ding, J. B. Nicholas, D. A. Dixon and L. S. Wang, *J. Phys. Chem. A*, 1999, **103**, 3423–3429.
27 G. Grégoire, M. Mons, I. Dimicoli, C. Dedonder-Lardeux, C. Jouvet, S. Martrenchard and D. Solgadi, *J. Chem. Phys.*, 2000, **112**, 8794–8805.
28 C. Dedonder-Lardeux, G. Grégoire, C. Jouvet, S. Martrenchard and D. Solgadi, *Chem. Rev.*, 2000, **100**, 4023–4038.
29 J. J. Max and C. Chapados, *J. Chem. Phys.*, 2001, **115**, 2664–2675.
30 A. Mizoguchi, Y. Ohshima and Y. Endo, *J. Am. Chem. Soc.*, 2003, **125**, 1716–1717.
31 Q. Zhang, C. J. Carpenter, P. R. Kemper and M. T. Bowers, *J. Am. Chem. Soc.*, 2003, **125**, 3341–3352.
32 A. T. Blades, M. Peschke, U. H. Verkerk and P. Kebarle, *J. Am. Chem. Soc.*, 2004, **126**, 11995–12003.
33 X. B. Wang, H. K. Woo, B. Jagoda-Cwiklik, P. Jungwirth and L. S. Wang, *Phys. Chem. Chem. Phys.*, 2006, **8**, 4294–4296.
34 Y. Feng, M. Cheng, X. Y. Kong, H. G. Xu and W. J. Zheng, *Phys. Chem. Chem. Phys.*, 2011, **13**, 15865–15872.
35 R. Z. Li, C. W. Liu, Y. Q. Gao, H. Jiang, H. G. Xu and W. J. Zheng, *J. Am. Chem. Soc.*, 2013, **135**, 5190–5199.
36 C.-W. Liu, G.-L. Hou, W.-J. Zheng and Y. Q. Gao, *Theor. Chem. Acc.*, 2014, **133**, 1550.
37 G. Feng, G. L. Hou, H. G. Xu, Z. Zeng and W. J. Zheng, *Phys. Chem. Chem. Phys.*, 2015, **17**, 5624–5631.
38 W. J. Zhang, G. L. Hou, P. Wang, H. G. Xu, G. Feng, X. L. Xu and W. J. Zheng, *J. Chem. Phys.*, 2015, **143**, 054302.
39 Z. Zeng, G. L. Hou, J. Song, G. Feng, H. G. Xu and W. J. Zheng, *Phys. Chem. Chem. Phys.*, 2015, **17**, 9135–9147.
40 R.-Z. Li, G.-L. Hou, C.-W. Liu, H.-G. Xu, X. Zhao, Y. Q. Gao and W.-J. Zheng, *Phys. Chem. Chem. Phys.*, 2016, **18**, 557–565.
41 J. A. Cowan, *The biological chemistry of magnesium*, VCH, Cambridge, 1995.
42 L. F. Wan and D. Prendergast, *J. Am. Chem. Soc.*, 2014, **136**, 14456–14464.
43 C. K. Chan, Z. Ha and M. Y. Choi, *Atmos. Environ.*, 2000, **34**, 4795–4803.
44 X. Li, J. Dong, H. Xiao, P. Lu, Y. Hu and Y. Zhang, *Sci. China, Ser. B: Chem.*, 2008, **51**, 128–137.
45 C. D. Cappa, J. D. Smith, B. M. Messer, R. C. Cohen and R. J. Saykally, *J. Phys. Chem. B*, 2006, **110**, 5301–5309.
46 M. F. Bush, J. T. O'Brien, J. S. Prell, C.-C. Wu, R. J. Saykally and E. R. Williams, *J. Am. Chem. Soc.*, 2009, **131**, 13270–13277.
47 D. R. Carl and P. B. Armentrout, *ChemPhysChem*, 2013, **14**, 681–697.
48 B. Jagoda-Cwiklik, P. Jungwirth, L. Rulíšek, P. Milko, J. Roithová, J. Lemaire, P. Maitre, J. M. Ortega and D. Schröder, *ChemPhysChem*, 2007, **8**, 1629–1639.
49 L. Jiang, T. Wende, R. Bergmann, G. Meijer and K. R. Asmis, *J. Am. Chem. Soc.*, 2010, **132**, 7398–7404.
50 J. Paterová, J. Heyda, P. Jungwirth, C. J. Shaffer, Á. Révész, E. L. Zins and D. Schröder, *J. Phys. Chem. A*, 2011, **115**, 6813–6819.
51 J. W. DePalma, P. J. Kelleher, C. J. Johnson, J. A. Fournier and M. A. Johnson, *J. Phys. Chem. A*, 2015, **119**, 8294–8302.
52 Y.-H. Zhang and C. K. Chan, *J. Phys. Chem. A*, 2000, **104**, 9191–9196.
53 X. Zhang, Y. Zhang and Q. Li, *THEOCHEM*, 2002, **594**, 19–30.
54 Y.-H. Zhang, M. Y. Choi and C. K. Chan, *J. Phys. Chem. A*, 2004, **108**, 1712–1718.

55 S. Langer, R. S. Pemberton and B. J. Finlayson-Pitts, *J. Phys. Chem. A*, 1997, **101**, 1277–1286.
56 M. E. Gebel, B. J. Finlayson-Pitts and J. A. Ganske, *Geophys. Res. Lett.*, 2000, **27**, 887–890.
57 H. Shaka, W. H. Robertson and B. J. Finlayson-Pitts, *Phys. Chem. Chem. Phys.*, 2007, **9**, 1980–1990.
58 J.-H. Park, A. V. Ivanov and M. J. Molina, *J. Phys. Chem. A*, 2008, **112**, 6968–6977.
59 J.-H. Park, C. I. Christov, A. V. Ivanov and M. J. Molina, *Geophys. Res. Lett.*, 2009, **36**, L02802.
60 H. Ohtaki and T. Radnai, *Chem. Rev.*, 1993, **93**, 1157–1204.
61 J. A. Cowan, *BioMetals*, 2002, **15**, 225–235.
62 D. E. Draper, *RNA*, 2004, **10**, 335–343.
63 M. Boero, T. Ikeda, E. Ito and K. Terakura, *J. Am. Chem. Soc.*, 2006, **128**, 16798–16807.
64 H.-G. Xu, Z.-G. Zhang, Y. Feng, J.-Y. Yuan, Y.-C. Zhao and W.-J. Zheng, *Chem. Phys. Lett.*, 2010, **2010**, 204–208.
65 J.-D. Chai and M. Head-Gordon, *Phys. Chem. Chem. Phys.*, 2008, **10**, 6615–6620.
66 M. J. Frisch, G. W. Trucks, H. B. Schlegel, G. E. Scuseria, M. A. Robb, J. R. Cheeseman, G. Scalmani, V. Barone, B. Mennucci, K. A. Peterson, H. Nakatsuji, M. Caricato and X. Li, *Gaussian 09, Revision A.01*, Gaussian, Inc., Wallingford, CT, 2009.
67 R. Krishnan, J. S. Binkley, R. Seeger and J. A. Pople, *J. Chem. Phys.*, 1980, **72**, 650–654.
68 L. Yang, C.-W. Liu, Q. Shao, J. Zhang and Y. Q. Gao, *Acc. Chem. Res.*, 2015, **48**, 947–955.
69 J. A. Pople, M. Head-Gordon and K. Raghavachari, *J. Chem. Phys.*, 1987, **87**, 5968–5975.
70 A. E. Reed, R. B. Weinstock and F. Weinhold, *J. Chem. Phys.*, 1985, **83**, 735–746.
71 E. D. Glendening, A. E. Reed, J. E. Carpenter and F. Weinhold, *NBO Version 3.1*, University of Wisconsin, Madison, Wisconsin, 1988.
72 J. Molnar, C. J. Marsden and M. Hargittai, *J. Phys. Chem.*, 1995, **99**, 9062–9071.
73 M. Pavlov, P. E. M. Siegbahn and M. Sandström, *J. Phys. Chem. A*, 1998, **102**, 219–228.
74 F. Misaizu, M. Sanekata, K. Fuke and S. Iwata, *J. Chem. Phys.*, 1994, **100**, 1161–1170.
75 M. Sanekata, F. Misaizu, K. Fuke, S. Iwata and K. Hashimoto, *J. Am. Chem. Soc.*, 1995, **117**, 747–754.
76 C. Berg, U. Achatz, M. Beyer, S. Joos, G. Albert, T. Schindler, G. Niedner-Schatteburg and V. E. Bondybey, *Int. J. Mass Spectrom. Ion Processes*, 1997, **167**, 723–734.
77 C. Berg, M. Beyer, U. Achatz, S. Joos, G. Niedner-Schatteburg and V. E. Bondybey, *Chem. Phys.*, 1998, **239**, 379–392.
78 B. M. Reinhard and G. Niedner-Schatteburg, *Phys. Chem. Chem. Phys.*, 2002, **4**, 1471–1477.
79 B. M. Reinhard and G. Niedner-Schatteburg, *J. Chem. Phys.*, 2003, **118**, 3571–3582.
80 C.-K. Siu and Z.-F. Liu, *Phys. Chem. Chem. Phys.*, 2005, **7**, 1005–1013.
81 M. K. Beyer, *Mass Spectrom. Rev.*, 2007, **26**, 517–541.
82 C. van der Linde, A. Akhgarnusch, C.-K. Siu and M. K. Beyer, *J. Phys. Chem. A*, 2011, **115**, 10174–10180.
83 T.-W. Lam, C. van der Linde, A. Akhgarnusch, Q. Hao, M. K. Beyer and C.-K. Siu, *ChemPlusChem*, 2013, **78**, 1040–1048.
84 G.-L. Hou, C.-W. Liu, R.-Z. Li, H.-G. Xu, Y. Q. Gao and W.-J. Zheng, *J. Phys. Chem. Lett.*, 2017, **8**, 13–20.
85 K. W. Oum, M. J. Lakin, D. O. DeHaan, T. Brauers and B. J. Finlayson-Pitts, *Science*, 1998, **279**, 74–77.
86 B. S. Fox, O. P. Balaj, I. Balteanu, M. K. Beyer and V. E. Bondybey, *J. Am. Chem. Soc.*, 2002, **124**, 172–173.
87 B. S. Fox, M. K. Beyer, U. Achatz, S. Joos, G. Niedner-Schatteburg and V. E. Bondybey, *J. Phys. Chem. A*, 2000, **104**, 1147–1151.